JOURNAL OF GEOPHYSICAL RESEARCH, VOL. 104, NO. C6, PAGES 13,605–13,613, JUNE 15, 1999

Rafting and ridging of thin ice sheets

Mark A. Hopkins

U.S. Army Cold Regions Research and Engineering Laboratory, Hanover, New Hampshire

Jukka Tuhkuri and Mikko Lensu

Ship Laboratory, Helsinki University of Technology, Espoo, Finland

Abstract. Rafting and pressure ridging are important processes in the deformation of sea ice that occur when two ice sheets are pushed together. In this study a two-dimensional computer model of the rafting and ridging process is used to simulate a situation in which two identical ice sheets are pushed together at constant speed. Each model ice sheet is composed of two thicknesses of ice. The ratio of the thicknesses is varied to obtain degrees of inhomogeneity. The accuracy of the simulations is assessed by comparison with a series of similar physical experiments performed in a refrigerated basin. Following this comparison, the computer model is used to perform an extensive series of simulations to explore the effect of the thickness and the thickness inhomogeneity of the model ice sheets on the likelihood of occurrence of ridging and rafting. During the simulations the energy consumption and forces are explicitly calculated. The energy consumed during the simulations is used to demonstrate the smooth transition between ridging and rafting that occurs when the homogeneity of the sheets is varied.

1. Introduction

The mechanical deformation of the ice cover in northern seas takes place through pressure ridging and rafting. Pressure ridges are the piles of ice rubble that criss-cross the ice pack. Ridges are created by the flexural failure of opposing ice sheets and subsequent piling of the ice blocks created by the flexural failure on top of and beneath the two sheets. Rafting is the simple overriding of one sheet by another sheet, resulting in a local doubling of ice thickness [*Parmerter*, 1975]. The study of the energetics and mechanics of the ridging and rafting processes is important because the energy expended in deformation determines the large-scale strength of the ice pack and because the strength and thickness of pressure ridges and rafted ice are important in the design and operation of arctic vessels and offshore structures.

Numerical modeling of pressure ridging began with the kinematic model of *Parmerter and Coon* [1972]. A dynamic model of the ridging process was developed by *Hopkins et al*. [1991]. This model, based on a two-dimensional particle simulation, considered the compression of a rubble-filled lead between multiyear floes. *Hopkins* [1994] developed another dynamic model of pressure ridge formation, in which an intact sheet of thin lead ice was pushed at constant speed against a thick multiyear floe. The thin sheet, breaking repeatedly in flexure, created the rubble blocks that form the ridge sail and keel. This study demonstrated the importance of friction as a dissipative mechanism and, less obviously, in controlling the relative volumes of the ridge sail and keel. This work was extended by *Hopkins* [1998] to look at the evolution of the ridge profile, ridge-building forces, and energetics as a function of lead ice thickness and the amount of lead ice pushed into the ridge. The current work extends these studies by considering ridging between identical sheets. Since both *Hopkins* [1994] and *Hopkins* [1998] were studies of pressure ridging, rafting events, which occurred in a small percentage of the simulations, were not reported. The low frequency of rafting events in these simulations was due to the large difference between the thicknesses of the lead ice sheet and multiyear floe.

Rafting has not received as much attention in the literature as pressure ridging. Perhaps this is because ridge keels are a greater concern for engineers or perhaps because, unlike ridging, it is trivial to calculate rafting forces, given an estimate of the coefficient of friction between the sheets. The difficult challenge is to determine under what conditions rafting should occur and not ridging. *Weeks and Kovacs* [1970], who show many examples of ridged and rafted ice, postulate a gradual transition between ridging and rafting processes which depends on the thickness of the sheets. The examples of rafting that they cite seem to occur between sheets of similar thickness. An analytical model of the initiation of rafting was developed by *Parmerter* [1975]. On the basis of the geometry of the opposing ends of the two ice sheets, he calculated the force required to initiate rafting. He compared the bending stress with the ice strength to determine whether rafting or breaking would occur. He found that the likelihood of rafting decreased with increasing modulus and thickness. However, dynamic effects at the leading edge of the sheets can create conditions under which similar sheets of any thickness can raft. First, when two ice sheets are pushed together, the geometry of the ends of the sheets can be changed by abrasion and crushing. Second, rubble created between the sheets can lift one sheet above the other. To put the argument another way, two ice sheets do not have just one chance to raft: they can continue to butt together, breaking and abrading, until conditions are right for rafting.

Rafting begins when one sheet overrides the other and progresses until the frictional force between the sheets, which increases linearly with the amount of overlap, arrests motion or causes buckling. The frictional force that resists the advance of the sheets is proportional to the product of the difference

Paper number 1999JC900031.
0148-0227/99/1999JC900031$09.00

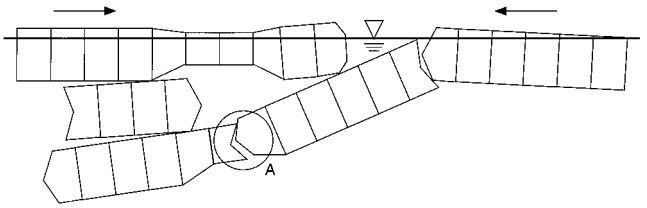

Figure 1. Showing the discretization of the computer model ice sheets into uniform rectangular blocks.

between the unit weight and buoyancy of either sheet and the length of the overlap between the sheets. In simulations of ridging between relatively thin first-year ice and a multiyear floe, the lead ice overrode the floe [*Hopkins*, 1994, 1998]. Because of the great buoyancy of the floe the lead ice sheet was lifted from the water, the rafting force rose rapidly, and, consequently, the sheets were unable to progress more than 10 or 20 m. In addition, the large degree of curvature required of the lead ice sheet in mounting the floe facilitated buckling, which also helped to terminate the rafting event. In contrast, in rafting between sheets of roughly equal thickness, the unit buoyancy of the submerged ice sheet is much less and curvature is less. Therefore the rafting force increases more slowly, and rafting progresses much farther. *Weeks and Anderson* [1958] describe a rafting episode 600 m in length.

In this study we consider rafting and ridging between two identical sheets. We began by trying to simulate ridging between identical sheets of uniform thickness. It quickly became apparent that rafting was the preferred mode between uniform sheets. Even simulations with rather thick sheets (0.5–0.9 m), which began by creating rubble, tended to raft as one sheet was lifted by the rubble. Concurrent ice basin model tests by *Tuhkuri and Lensu* [1998], in which two identical ice sheets were pushed together, also showed that uniform ice sheets tend to raft. Our attention moved to thickness inhomogeneity as the factor that determines the relative likelihood of ridging and rafting between identical ice sheets. In this study we push together two identical model ice sheets each composed of two thicknesses, as shown in Figure 1. In nature an ice sheet composed of two thicknesses might be created from the breaking, dilating, and refreezing of a uniform sheet. Two pressure ridges formed from composite ice sheets of this type were studied during a recent field experiment in the Gulf of Bothnia [*Lensu et al*., 1998].

We obtained degrees of inhomogeneity by varying the two thicknesses of ice in the sheet. We use the ratio obtained by dividing the thickness of the thinner ice by the thickness of the thicker ice to describe the inhomogeneity of the ice sheet. In the simulations we varied the ratio between 2/8 (highly inhomogeneous ice) and 8/8 (homogeneous ice). By decreasing the ratio of the thickness of the thinner ice to the thicker ice in simulations, it was possible to obtain the consistent rubble formation necessary for ridging. In the region between highly inhomogeneous ice (2/8) and homogeneous ice (8/8), where the probable occurrence of ridging or rafting is variable, we identify smoothly varying transitional behavior.

2. Dynamic Computer Model of Ridging and Rafting

The ridging/rafting model is based on a computer program that simulates the dynamics of a system of discrete, two-dimensional ice blocks. The position, orientation, velocity, and shape of each block are stored in arrays. At each time step the contact and body forces on each block are calculated, and the blocks are moved to new locations with new velocities that depend on the resultant of the forces. The simulations begin with the collision of two floating model ice sheets pushed together at a constant speed. Blocks are broken from the sheets through flexural failure (including buckling) at points where tensile stress exceeds strength. The blocks of rubble broken from the sheets may undergo secondary flexural breakage. The forces at contacts between rubble blocks and between rubble blocks and the sheets have inelastic and frictional components. Buoyancy of the model ice sheets and rubble blocks and water drag are also modeled. The mechanical details of the model, which are largely the same as from *Hopkins* [1994], are summarized here.

The model ice sheets are composed of single rows of rectangular blocks that are attached to neighboring blocks by viscous-elastic joints. The discretization of the sheet and rubble blocks is shown in Figure 1. The boundary conditions on the sheets, in the form of global damping, are discussed by *Hopkins* [1994]. Relative displacements between adjacent component blocks create forces and moments, internal to the sheet and rubble blocks. The internal forces on the component blocks are added to external forces exerted by the surrounding ice rubble, gravity, and buoyancy. When the tensile stress in a joint at either surface of a sheet or rubble block exceeds the specified strength, a crack is initiated. The crack propagates at constant speed (10 m s^{-1}) across the joint, requiring many time steps Δt $O(10^{-4}$ s) for completion. The block created by the fracture becomes part of the rubble and is added to the ridge structure. While the cracks must occur at joints, the length of the rubble blocks is variable since they may contain any number of component blocks.

Because of the two dimensionality of the model ice sheets, there is little continuity across a crack between two blocks. A real ice sheet is able to maintain continuity, in spite of the presence of flexural cracks, as long as the curvature is small. This is probably due to the nonuniformity of the surface of the crack. To introduce similar continuity into the two-dimensional ice sheet model, a shallow socket was created at broken joints. The depth of the socket used in the simulations was 15% of the ice sheet thickness at the joint. A socket is shown at A in Figure 1. As long as the joint remains under compression, the two blocks remain together, but when the compression is removed, the blocks are free to separate.

Contact forces between rubble blocks and between rubble and sheet use a force model that supports no tensile force. Two blocks are defined to be in contact if the polygons defining their shapes intersect. The intersection is interpreted as a deformation of the blocks resulting in a contact force. The contact force has components normal **n** and tangential **t** to a contact surface connecting the intersection points. The force acts at the centroid of the area of intersection. The normal component of the contact force is

$$F_n^n = -k_n A^n - \eta \mathbf{V}_{1/2} \cdot \mathbf{n} \quad (1)$$

The subscript n denotes the normal direction, the superscript n denotes the current time step, k_n is the normal contact stiffness, A^n is the area of intersection of the blocks, η is the normal contact viscosity, and $\mathbf{V}_{1/2}$ is the relative velocity of block 1 with respect to block 2 at the point of contact. A value of η near critical damping is used to produce highly inelastic

Figure 2. Snapshot of a ridging experiment in the ice basin at the Helsinki University of Technology.

behavior. Tensile forces are not modeled. The incremental change in the tangential force due to friction is proportional to the relative tangential velocity. The tangential force at time n is

$$F_t^n = F_t^{n-1} - k_t \Delta t \mathbf{V}_{1/2} \cdot \mathbf{t} \tag{2}$$

where Δt is the time step and k_t is the tangential contact stiffness that is set to 60% of k_n. If the tangential force F_t exceeds the Coulomb limit, μF_n, where μ is the friction coefficient, it is scaled such that $F_t = \mu F_n$. The moments on each floe are calculated from the forces and moment arms. A simple water drag and a buoyant force on each block are also calculated. After the sums of the forces and moments exerted on each block have been calculated, the equations of motion are solved using simple central difference approximations and time advanced.

The ridging or rafting force is the sum of the horizontal forces opposing the motion of each sheet. A force sufficient to push the sheets at a constant speed is assumed to be available. The work done by the moving sheets, the change in the kinetic and potential energy of the blocks, and the energy dissipated by inelastic and frictional contacts and water drag are calculated at each time step. Inelastic and frictional dissipations are determined by computing the work performed by the normal and tangential components of each contact force. These calculations are described by *Hopkins* [1994]. The energy balance is used to gauge the numerical accuracy of the simulation. In the simulations described in sections 3 and 4, the error in the energy balance was $<1\%$.

3. Comparisons Between Simulations and Basin Experiments

A series of physical experiments, three-dimensional versions of the two-dimensional discrete element simulations, were performed in the 40×40 m square ice basin at the Ship Laboratory of the Helsinki University of Technology. A uniform sheet of model ice was grown over the entire basin. Three rectangular samples 6 m wide and 26 m long were created in the ice cover. Slots were cut along the 26 m long edges and across the center of each sample, dividing it into two sheets. The ice at one end was left attached to the parent sheet. During the experiments the two sheets were confined on three sides by the parent ice sheet and on the fourth side by a vertical pusher plate attached through load cells to a movable carriage. In the experiments the pusher plate moved about 12 m at a constant speed. The force on the pusher plate was measured at 12 Hz.

The experiments using uniform ice sheets invariably resulted in the occurrence of simple rafting, where one sheet overrides the other along a linear front for the duration of the test [*Tuhkuri and Lensu*, 1998]. To create ridges, it was necessary to use inhomogeneous ice sheets. A simple nonuniform sheet was constructed by cutting the ice sheet in each sample into 500 mm square floes and mixing them. Since none of the floes were discarded prior to mixing, some rafting necessarily occurred during the mixing process. After mixing the floes, the ice sheet was refrozen by spraying a second layer of ice over the broken ice field. The experimental ice field is shown in Figure 2. The final thickness of the ice sheet, which is the same as the average thickness $\langle h \rangle$, was the sum of the thickness of the initial ice sheet and the second layer added during refreezing. Since the amount of rafted ice was relatively small, the sheet essentially consisted of two thicknesses; thick ice h_1 equal to the average thickness and thin ice h_2 equal to the thickness of the second layer added during refreezing.

Seventeen experiments were performed using nonuniform ice sheets. Ridging occurred in all of the experiments except one. Typically, part of the 6 m wide moving sheet dove under the stationary sheet, while the remainder overrode the stationary sheet. As the tests progressed, the deformation zones at the leading edges of the overriding sheets assumed a sinusoidal appearance. The serpentine shape can be seen in Figure 2. The light color of the band of ice surrounding the ridge line is caused by the presence of the underwater ridge keel. Following each experiment, several cross-sectional cuts were made through the ridge to measure the keels. The one experiment that resulted in simple rafting was used to determine the coefficient of sliding friction of the composite sheet.

Table 1. Parameters Used in the Physical Experiments

Parameter	Value
$\langle h \rangle$ (average ice thickness)	68 mm
h_1 (thickness of thick ice)	68 mm
h_2 (thickness of thin ice)	24 mm
ice sheet speed	10 mm s^{-1}
floe size	500 × 500 mm
E (modulus)	60 MPa
σ_f (downward breaking)	46 kPa
σ_f (upward breaking)	38 kPa
ρ_i (ice density)	930 kg m^{-3}
ρ_w (water density)	1000 kg m^{-3}
μ (sliding friction)	0.41

Eight simulations were performed using the computer model described above. Ridging occurred in all eight simulations. The material parameters used in the simulations were the same as in Table 1. The model ice sheets used in the simulations were 70% 75 mm thickness and 30% 47 mm thickness for an average thickness of 67 mm. The sections of thin ice were randomly distributed throughout the sheet. The speed of the sheets was constant. The rate of convergence of the ice sheets was increased to 50 mm s^{-1} to reduce computational time. Simulations at lower speeds showed no systematic velocity related effects. The normal contact stiffness for rubble contacts k_n was 1 MPa. The tangential stiffness coefficient k_t was 60% of the normal value. The normal viscosity coefficient η was set to 50% of the critical damping value $2(k_n\langle h \rangle \rho_i)^{1/2}$ to produce highly inelastic behavior in collisional contacts. A random variation (±5%) in the elastic modulus at each joint in the ice sheet was used to create unique outcomes in simulations using the same initial configuration of the ice sheet and the same set of parameters. This small variation was sufficient to cause the simulations to diverge noticeably by the time several blocks had been broken from the parent sheets. This does not imply extreme sensitivity to the elastic modulus but, rather, the chaotic nature of the process.

The rafting force F_r is the force acting in the horizontal plane to push the sheets together and is primarily a result of the frictional contact at the interface between the two sheets. The frictional component of F_r depends on the upward acting net buoyancy of the bottom sheet and the coefficient of sliding friction μ between the sheets. The rafting force increases linearly in proportion to the relative displacement D of the sheets. The rafting force also has a constant component F_0 that is due to the curvature of the sheets, which is greatest in the vicinity of the leading edge of the top sheet, and to the tearing of the sheets at the node between the fingers in the basin experiments. The equation for the rafting force (per meter of width) is

$$F_r = F_0 + \mu(\rho_w - \rho_i)\, g\langle h \rangle D \tag{3}$$

where g is the acceleration of gravity and $\langle h \rangle$ is the mean ice thickness. The friction coefficient μ in Table 1 was obtained by fitting (3) to a plot of force versus displacement in the one physical experiment that rafted. The rafting work W_r, obtained by integrating (3), is

$$W_r = F_0 D + \tfrac{1}{2}\mu(\rho_w - \rho_i)\, g\langle h \rangle D^2 \tag{4}$$

The forces calculated during the entire group of eight simulations, averaged over 1 s intervals, are shown in Figure 3. The corresponding rafting force from (3), using the parameter values listed in Table 1, is shown by a dashed straight line. The rafting force tightly bounds the simulation results over the tested range of deformation, in spite of the fact that all eight simulations ridged. Typical force/displacement curves from a single simulation and a single experiment are shown in Figure 4. The simulation force record in Figure 4 is characterized by several episodes in which the force rises to near the rafting level, remains for a short while, and then drops precipitously. These extreme oscillations, found in all eight simulations, are caused by the two dimensionality of the computer model. This is because after the leading end of the sheet fails either by buckling or bending, the remainder of the sheet is completely unloaded and the force drops to zero. In contrast, the graph of

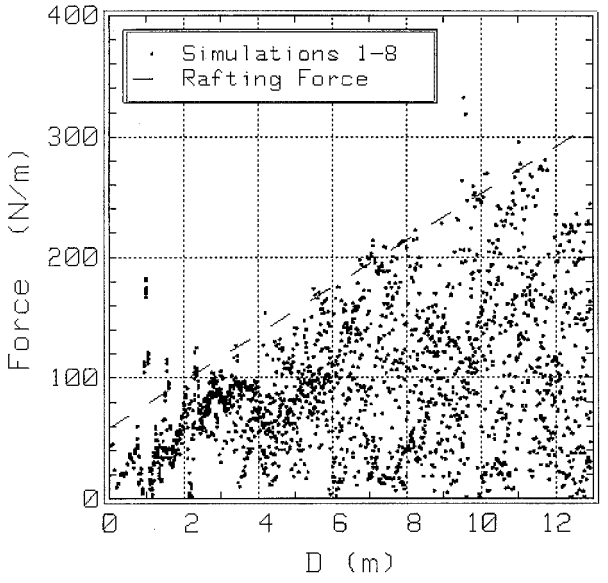

Figure 3. Instantaneous force data from eight simulations. The dashed line is the rafting force given by (3).

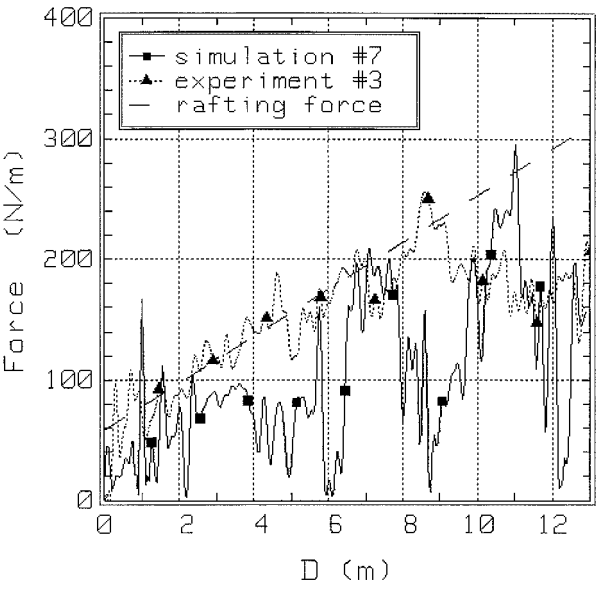

Figure 4. Force versus displacement from a typical simulation and a typical experiment. The dashed line is the rafting force given by (3).

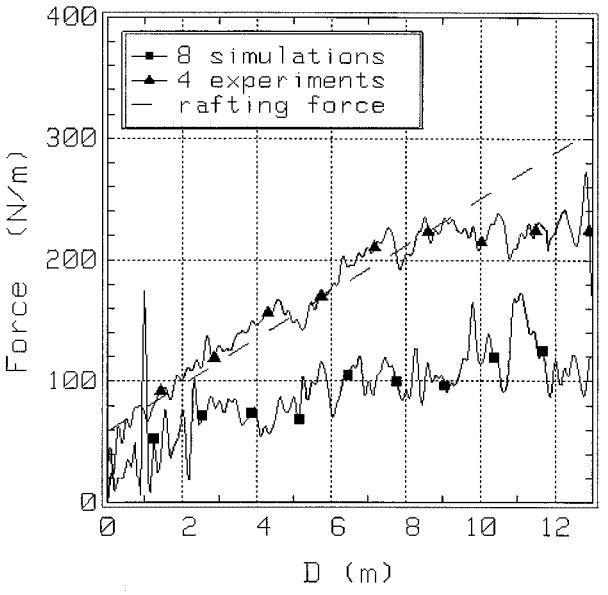

Figure 5. Comparison between the average force from four experiments and the average force from eight simulations. The dashed line is the rafting force given by (3).

the force from the physical experiment displays small oscillations that reflect the many small, nonsimultaneous failure events taking place at the leading edge of the 6 m wide (about nine characteristic lengths) sheets. For this reason, the complete unloading observed in the simulation graph, characteristic of the two-dimensional model, is not a general feature of the force graphs from the three-dimensional physical experiments. A second feature that tended to minimize large force oscillations in the physical experiments is the way in which the inhomogeneous sheets were constructed. The sheets were cut into 500 mm square pieces that were mixed up and refrozen. By mixing the square pieces, the joints of thin ice between the square pieces were staggered rather than running across the sheet. This method of construction strengthens the sheet and, while it is certainly more realistic in terms of what one would expect to find in the field, weakens the direct comparison with the two-dimensional simulations. In a two-dimensional model sheet, which by definition is uniform in the third dimension, the joints of thin ice run straight across the entire sheet.

The graphs of the average force from four representative physical experiments and the simulations are shown in Figure 5. The one experiment that rafted is not included. The straight dashed line in Figure 5 is the rafting force (3) with the parameter values listed in Table 1. The average force from the simulations is approximately one-half the level measured in the physical experiments. The rafting force (3) remains the upper limit on the ridging forces. Although there is a significant quantitative difference in the average force levels, we believe that the correspondence between the simulation and experimental results is sufficiently close to justify using the computer model to study the qualitative effect of ice thickness inhomogeneity on the ridging/rafting process.

4. A Parameter Study Using Simulations

The main parameters that determine the likelihood of rafting and ridging appear to be the elastic modulus and the thickness identified by *Parmerter* [1975] and thickness inhomogeneity introduced here. Inhomogeneity is modeled in the simulations by defining a standard ice sheet composed of two thicknesses having 70% thicker ice h_1 and 30% thinner ice h_2. The average ice thickness $\langle h \rangle$ equals $0.7h_1 + 0.3h_2$. The thinner ice was randomly distributed along the sheet. This is meant to suggest a scenario in nature in which an ice sheet is broken, dilated, and refrozen. To determine the effect of ice thickness inhomogeneity on the ridging/rafting process, we performed simulations with the computer model for five values of the major ice thickness h_1 and seven values of the ratio of the minor to major ice thickness h_2/h_1. Seven simulations were performed with each pair of thicknesses. The parameters used in the simulations are listed in Table 2.

Table 2. Parameters Used in the Simulations

Parameter	Value
h_1 (major thickness)	0.1, 0.3, 0.5, 0.7, 0.9 m
h_2/h_1 (thickness ratio)	2/8 to 8/8
u_s (combined ice speed)	0.1 m s^{-1}
W (sheet block width)	1/5 of characteristic length L_c
E modulus	3 GPa
ν (Poisson's ratio)	0.3
Tensile strength (ice top)	750 kPa
Tensile strength (ice bottom)	350 kPa
ρ_i (ice density)	920 kg m^{-3}
ρ_w (water density)	1010 kg m^{-3}
μ (friction coefficient)	0.4
k_n (normal contact stiffness)	10^8 N m^{-3}

In each simulation the total relative displacement of the opposing ice sheets was 15 characteristic lengths. The characteristic length of the composite ice sheets L_c, from the theory of beams on an elastic foundation [*Hetenyi*, 1946], was defined in terms of the average ice thickness $\langle h \rangle$ as

$$L_c = \sqrt[4]{\frac{E\langle h \rangle^3}{12\rho_w g}} \tag{5}$$

The range of average thicknesses $\langle h \rangle$ and characteristic lengths L_c for the various major thicknesses h_1 and ratios h_2/h_1 used in the simulations are compared in Table 3. The $15L_c$ column shows the total relative displacement of the ice sheets in simulations with the indicated pair of ice thicknesses.

Simulations using homogeneous sheets ($h_1 = h_2 = \langle h \rangle$) had a high probability of rafting. When the thickness ratio h_2/h_1 was reduced, increasing the nonuniformity of the sheet, the probability of rafting decreased and the probability of ridging increased. A snapshot from a simulation that rafted, with a thickness ratio of 8/8, is shown in Figure 6. A snapshot from a simulation that ridged, with a thickness ratio of 3/8, is shown in Figure 7. In the region between uniform ice (8/8) and highly nonuniform ice (2/8), where the probable occurrence of ridging or rafting was variable, the outcome of a simulation might be a combination of the two. A snapshot showing a combination of ridging and rafting, from a simulation with a thickness ratio of 6/8, is shown in Figure 8. Transitional behavior is evident in the forces and energy consumption measured in the simulations.

In the following figures the relative displacement D was nondimensionalized by the characteristic length L_c, and the force F and the work W were nondimensionalized by the dominant components of the rafting force (3) and the rafting work (4) at a displacement of $D = 15L_c$ as

Table 3. Average Ice Thicknesses and Characteristic Lengths for Various Thicknesses and Thickness Ratios

h_1, m	$\langle h \rangle$ (8/8), m	$\langle h \rangle$ (2/8), m	L_c (8/8), m	L_c (2/8), m	15 L_c (8/8), m
0.1	0.1	0.08	2.24	1.85	33.6
0.3	0.3	0.23	5.11	4.22	76.6
0.5	0.5	0.39	7.49	6.19	112.4
0.7	0.7	0.54	9.65	7.97	144.7
0.9	0.9	0.70	11.65	9.68	174.7

$$D^* = D/L_c$$

$$F^* = F/[\mu(\rho_w - \rho_i)g\langle h \rangle(15L_c)] \quad (6)$$

$$W^* = W/[\tfrac{1}{2}\mu(\rho_w - \rho_i)g\langle h \rangle(15L_c)^2]$$

The effectiveness of the nondimensionalization is demonstrated in Figure 9, in which the nondimensional work versus displacement graphs for five major ice thicknesses essentially collapse to a single graph.

Force versus displacement graphs from simulations using $h_1 = 0.3$ m and ratios from 2/8 to 8/8 are shown in Figure 10. Each graph is the average of the results of seven simulations. Each graph was smoothed using a low pass filter. Although Figure 10 is cluttered, it is clear that the forces increase with the thickness ratio h_2/h_1. The graph for the thickness ratio of 8/8 closely approximates the nondimensional rafting force, which increases linearly with displacement. The other graphs that fill in the area below the rafting force are from simulations in which progressively greater amounts of ridging occurred. The forces tend to increase with the thickness ratio because (1) the probability of rafting increases and (2) rafting forces are higher than ridging forces.

Work versus displacement graphs from the same series of simulations are shown in Figure 11. The graphs were obtained by integrating the average forces in Figure 10. The work increases with the thickness ratio for the same reasons given above. The smooth increase in the work versus displacement graphs with increasing thickness ratio shows that the transition from ridging to rafting is quite seamless. Graphs of work versus displacement for the other four major ice thicknesses appear quite similar. Rather than present four graphs we show instead, in Figure 12, a contour plot of W^* at $D^* = 15$ for each major thickness and thickness ratio. Each value of W^* is an average of seven simulations. Lower values of W^* denote a high probability of ridging, and higher values denote a high probability of rafting. Figure 12 shows that ridging tends to occur in thicker and more inhomogeneous ice sheets, while rafting tends to occur in thinner and more homogeneous sheets. Figure 12 also shows that while thin, fairly homogeneous sheets always raft, thick, homogeneous sheets are also quite likely to raft. However, as was mentioned above, rafting of thick sheets may be preceded by a period of rubbling before conditions are right for rafting.

The ratio of work to potential energy is an important variable in large-scale sea ice models [*Flato and Hibler*, 1995], where it is used to parametrize total energy losses in terms of the change in potential energy due to deformation. The ratio of work to potential energy as a function of the major thickness and thickness ratio (for $D^* = 15$) is shown in Figure 13. The data points are averages of seven simulations with each pair of thicknesses. The ratio of work to potential energy found by *Hopkins* [1998] for ridging between first-year ice and a multiyear floe ranged from 9 to 14 for $D^* = 15$. The very high values of $W/\Delta PE$ shown in Figure 13 for the larger thickness ratios reflect a high proportion of rafting events. Rafting events have much higher ratios of work to potential energy because rafting requires more work and results in a very small increase in potential energy.

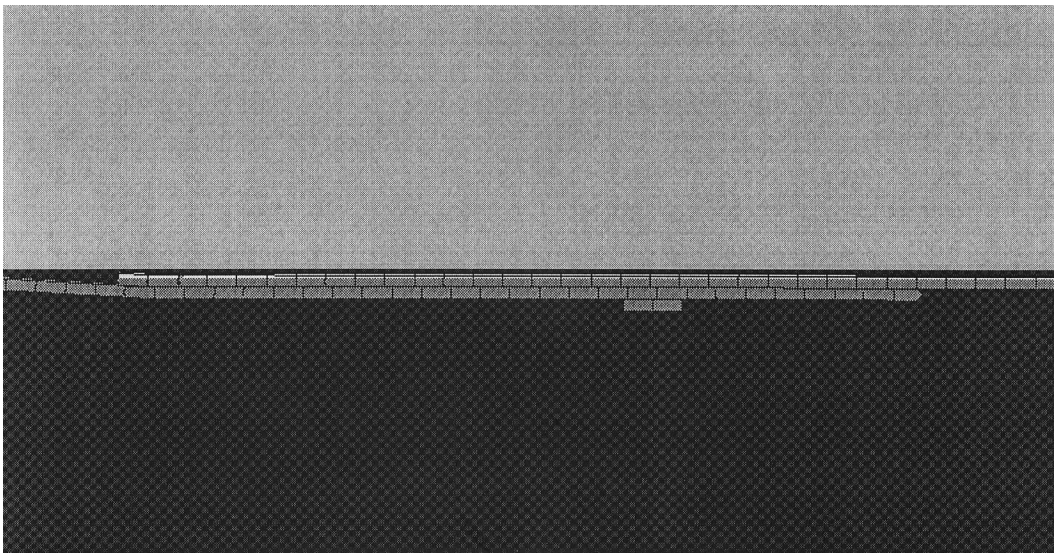

Figure 6. Scene from a simulation showing rafted sheets with major thickness $h_1 = 0.3$ m and a thickness ratio of 8/8.

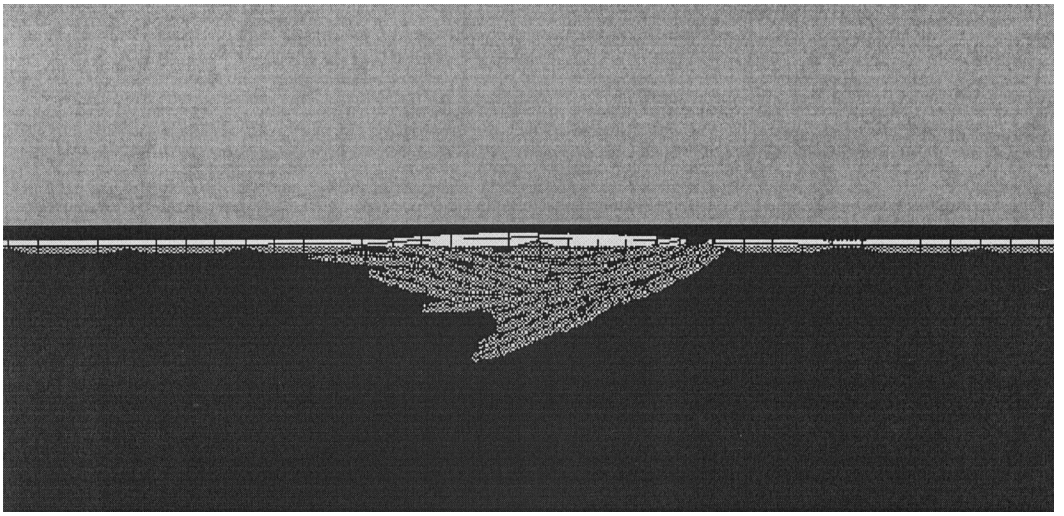

Figure 7. Scene from a simulation showing ridged ice with major thickness $h_1 = 0.3$ m and a thickness ratio of 3/8.

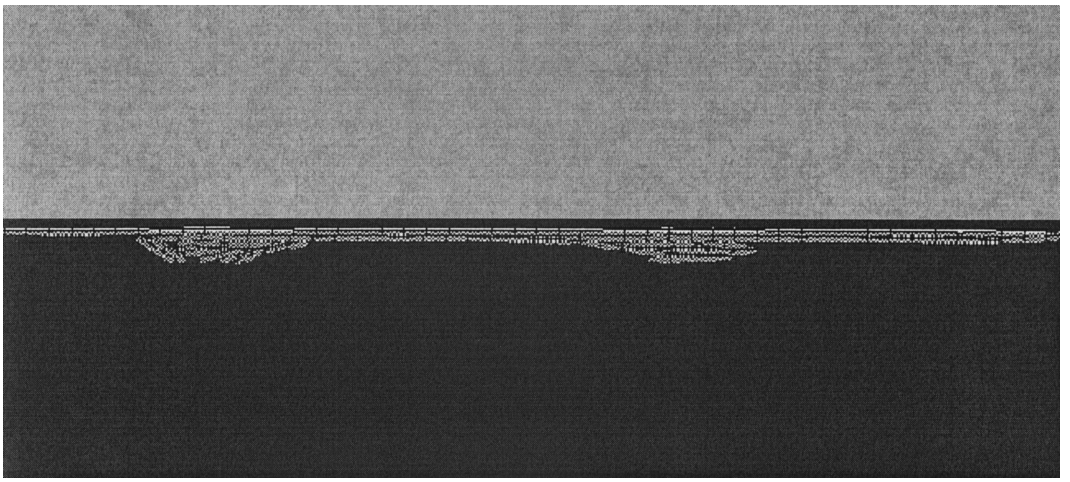

Figure 8. Scene from a simulation showing transitional behavior, which is a combination of ridged ice and rafted ice, with major thickness $h_1 = 0.3$ m and a thickness ratio of 6/8.

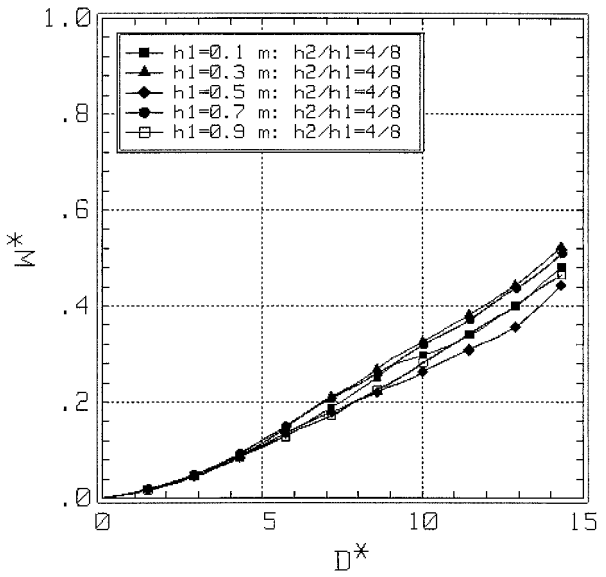

Figure 9. Nondimensional work versus nondimensional displacement from simulations in which the major thickness h_1 is varied while the thickness ratio is held constant.

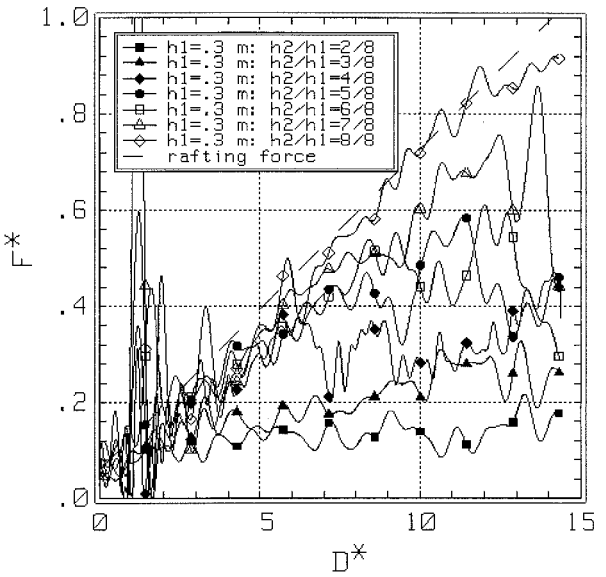

Figure 10. Nondimensional force versus nondimensional displacement from simulations in which the major thickness h_1 is held constant while the thickness ratio is varied from 2/8 to 8/8.

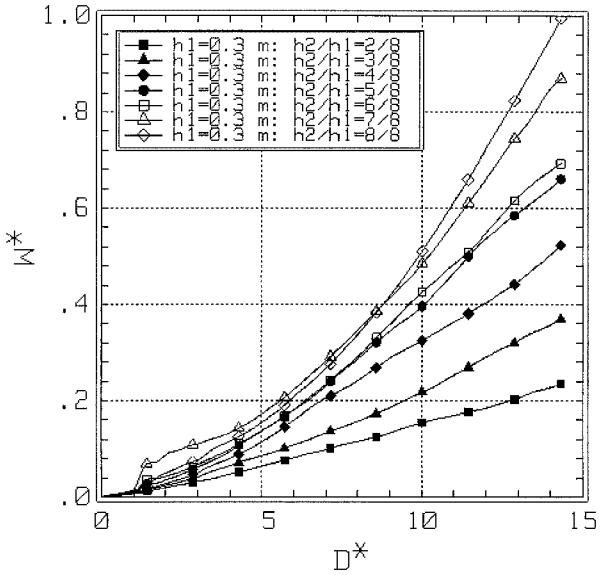

Figure 11. Nondimensional work versus nondimensional displacement from simulations in which the major thickness h_1 is held constant while the thickness ratio is varied from 2/8 to 8/8.

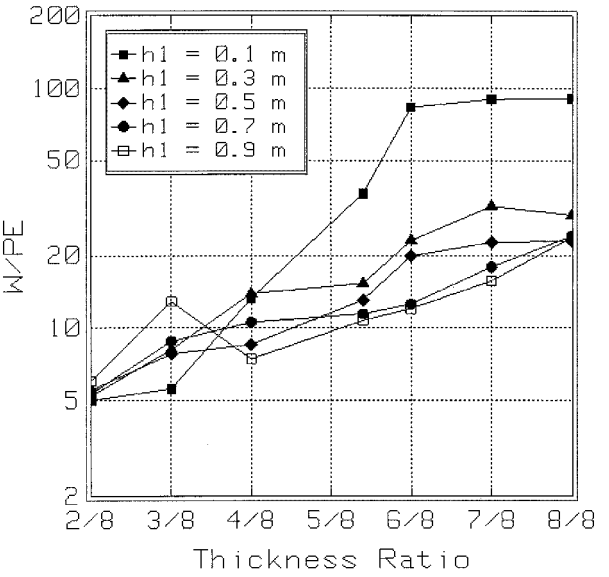

Figure 13. The ratio of work to potential energy as a function of the major ice thickness h_1 and the thickness ratio h_2/h_1 at a nondimensional displacement of $D^* = 15$.

5. Conclusions

In this study a two-dimensional computer model of the rafting and ridging process was developed and used to simulate a situation in which two identical sheets of ice are pushed together at constant speed. The range of outcomes found in the simulations shows that the thickness inhomogeneity of the ice sheets is an important parameter governing the likelihood of ridging and rafting along with the ice thickness and the elastic modulus identified by *Parmerter* [1975]. Thickness inhomogeneity was implemented in the computer model by using model ice sheets composed of fixed fractions of two ice thicknesses. A range of inhomogeneity was obtained by varying the ratio of the thickness of the thinner ice to the thicker ice from 2/8 to 8/8 (uniform ice) in seven steps. The simulations also show that the rafting and ridging process is not dependent on initial conditions. The alignment of the leading ends of the sheets changes continually due to rubble buildup beneath the ice sheets. This makes possible rafting between thick sheets and also means that rafting and ridging can alternate.

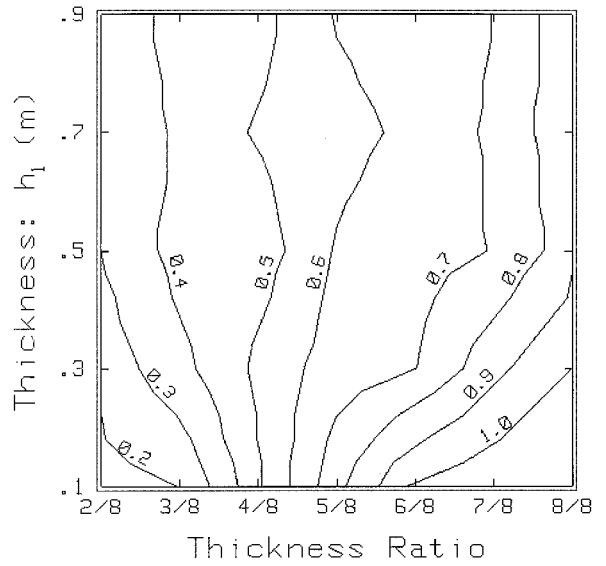

Figure 12. Contour plot of non-dimensional work W^* as a function of the major ice thickness h_1 and the thickness ratio h_2/h_1 at a nondimensional displacement of $D^* = 15$.

The results of the computer simulations were compared with the results of similar, three-dimensional physical experiments for a single average ice thickness and thickness ratio. All of the simulations and all but one of the experiments resulted in ridging. The comparison showed that the average simulation forces underestimated the average experimental forces by ~50%. The difference is most likely due to the two dimensionality of the computer model. Although the average simulation forces were significantly lower than the experimental forces, both sets of forces lay within the envelope defined by the graph of the rafting force versus ice sheet displacement. The results of this comparison, together with the results of further simulations, suggest that the rafting force is the upper bound on the ridging force for ridging that takes place between ice sheets of similar thickness.

Further simulations were performed with the computer model using model ice sheets of various thicknesses and degrees of thickness inhomogeneity to assess qualitatively the effect of thickness inhomogeneity on the ridging/rafting process. The simulations showed that ridging predominates at the low or inhomogeneous end of the thickness ratio and rafting predominates at the high or homogeneous end of the ratio. Mixed ridging and rafting behavior occurred in the region between the two extremes. Graphs of force versus displacement and work versus displacement were both found to increase with the thickness ratio. The progressive increase of force and work caused by increasing the thickness ratio points to a region of smooth transition from ridging to rafting. In the transitional region force and work increase with the thickness ratio because (1) rafting forces are higher than ridging forces and (2) the probability of rafting increases.

The outcomes of the simulations exhibit varying mixtures of rafting and ridging behavior, across the parameter space of

thickness and inhomogeneity. They range from simple rafting where there are just two layers of ice (Figure 6) to multiple layering to layering with some rubble creation (Figure 8) to ridging with some layering to pure ridging (Figure 7). In the transitional region between pure rafting and ridging, it is impossible to divide a mixed outcome into a ridging part and a rafting part. Therefore there is no basis for calculating a meaningful probability of ridging or rafting. The alternative is, as we do here, to characterize transitional behavior in terms of some measure of the process such as energy consumption.

Acknowledgments. The work described here is a part of the "Ice State" project supported by the European Commission through the Marine Science and Technology programme (MAST III). The participants in the project are Helsinki University of Technology, Nansen Environmental and Remote Sensing Center, Scott Polar Research Institute, University of Helsinki, and University of Iceland. Mark Hopkins' work was supported by a Secretary of the Army Research and Study Fellowship and by the Finnish Maritime Foundation.

References

Flato, G. M., and W. D. Hibler III, Ridging and strength in modeling the thickness distribution of Arctic sea ice, *J. Geophys. Res*., *100*, 18,611–18,626, 1995.

Hetenyi, M., *Beams on Elastic Foundations*, Univ. of Mich. Press, Ann Arbor, 1946.

Hopkins, M. A., On the ridging of intact lead ice, *J. Geophys. Res*., *99*, 16,351–16,360, 1994.

Hopkins, M. A., Four stages of pressure ridging, *J. Geophys. Res*., *103*, 21,883–21,891, 1998.

Hopkins, M. A., W. D. Hibler III, and G. M. Flato, On the numerical simulation of the sea ice ridging process, *J. Geophys. Res*., *96*, 4809–4820, 1991.

Lensu, M., J. Tuhkuri, and M. Hopkins, Measurements of curvilinear ridges in the Bay of Bothnia during the ZIP-97 experiment, *Rep. M-231*, 64 pp., Ship Lab., Helsinki Univ. of Technol., Espoo, Finland, 1998.

Parmerter, R. R., A model of simple rafting in sea ice, *J. Geophys. Res*., *80*, 1948–1952, 1975.

Parmerter, R. R., and M. D. Coon, Models of pressure ridge formation in sea ice, *J. Geophys. Res*., *77*, 6565–6575, 1972.

Tuhkuri, J., and M. Lensu, Ice tank tests on ridging of non-uniform ice sheets, *Rep. M-236*, Ship Lab., Helsinki Univ. of Technol., Espoo, Finland, 1998.

Weeks, W. F., and D. L. Anderson, Sea ice thrust structures, *J. Glaciol*., *3*, 173–175, 1958.

Weeks, W. F., and A. Kovacs, On pressure ridges, *CRREL Rep. IR505*, 1970.

M. A. Hopkins, U.S. Army Cold Regions Research and Engineering Laboratory, 72 Lyme Road, Hanover, NH 03755. (hopkins@crrel.usace.army.mil)

M. Lensu and J. Tuhkuri, Ship Laboratory, Helsinki University of Technology, Tietotie 1, FIN 02150, Espoo, Finland.

(Received June 15, 1998; revised January 25, 1999; accepted January 29, 1999.)